

Quasi-transverse electromagnetic modes supported by a graphene parallel-plate waveguide

George W. Hanson^{a)}

Department of Electrical Engineering, University of Wisconsin-Milwaukee, 3200 N. Cramer St., Milwaukee, Wisconsin 53211, USA

(Received 21 June 2008; accepted 4 September 2008; published online 29 October 2008)

A model is developed for a parallel-plate waveguide formed by graphene. The graphene is represented by an infinitesimally thin, local two-sided surface characterized by a surface conductivity obtained from the Kubo formula. Maxwell’s equations are solved for the model fields guided by the graphene layers. It is shown that despite the extreme thinness of its walls, a graphene parallel-plate waveguide can guide quasi-transverse electromagnetic modes with attenuation similar to structures composed of metals, while providing some control over propagation characteristics via the charge density or chemical potential. Given the interest in developing graphene electronics, such waveguides may be of interest in future applications. © 2008 American Institute of Physics. [DOI: 10.1063/1.3005881]

I. INTRODUCTION

Graphene, a two-dimensional version of graphite, consists of a planar atomic layer of carbon atoms bonded in a hexagonal structure. Intrinsic graphene is a zero bandgap semiconductor that is very promising for emerging nanoelectronic applications.¹ Graphene’s transport characteristics and conductivity can be tuned by either electrostatic or magnetostatic gating, or via chemical doping,^{2–4} leading to the possibility of various electronic devices.^{5,6} In addition, graphene is stable and extremely rigid and can exhibit ballistic transport over at least several hundred nanometers. A recent review of graphene physics is provided in Ref. 7.

In addition to dc transport devices, there has been considerable interest in developing graphene devices extending to microwave frequencies and beyond.^{8,9} Although it has only recently become possible to fabricate graphene,² currently graphene flakes larger than 100 μm are possible,¹⁰ with sizes continuing to grow as fabrication methods are refined and new methods are developed. Large-area graphene opens up the possibility of applications in the microwave and far-infrared regimes. Electromagnetic surface waves guided by graphene were considered in Refs. 9 and 11 and other electromagnetic field–graphene interactions were studied in Refs. 12–16.

In this work, a model is developed for the analysis of graphene sheets forming a parallel-plate waveguide (PPWG). The dominant, quasi-transverse electromagnetic (quasi-TEM) mode supported by the waveguide is studied, where it is shown that the modal field pattern, field confinement, and attenuation can be competitive with much thicker-walled ordinary metallic PPWGs at GHz and far-infrared frequencies. All units are in the SI system, and the time variation (suppressed) is $e^{j\omega t}$, where j is the imaginary unit.

II. ELECTROMAGNETIC MODEL OF GRAPHENE

Figure 1 depicts two laterally infinite graphene sheets spaced a distance d apart and immersed in a layered medium, where all material parameters may be complex valued. Each graphene sheet is modeled as an infinitesimally thin, local two-sided surface characterized by a surface conductivity. This model of graphene follows from the two-sided conductivity surface approach developed in Ref. 17 for carbon nanotubes, which was applied to local isotropic graphene in Ref. 11 and to nonlocal anisotropic graphene in Ref. 12. The conductivity σ can be determined from the Kubo formalism,¹⁸ and an explicit expression is¹⁹

$$\sigma(\mu_c) = \frac{je^2(\omega - j\tau^{-1})}{\pi\hbar^2} \times \left[\frac{1}{(\omega - j\tau^{-1})^2} \int_0^\infty \times \xi \left(\frac{\partial f_d(\xi, \mu_c, T)}{\partial \xi} - \frac{\partial f_d(-\xi, \mu_c, T)}{\partial \xi} \right) d\xi - \int_0^\infty \frac{f_d(-\xi, \mu_c, T) - f_d(\xi, \mu_c, T)}{(\omega - j\tau^{-1})^2 - 4(\xi/\hbar)^2} d\xi \right], \quad (1)$$

where ω is radian frequency, ξ is energy, μ_c is chemical potential, τ is a phenomenological electron relaxation time (τ^{-1} is the scattering rate) that is assumed to be independent of energy, $-e$ is the charge of an electron, \hbar is the reduced Planck’s constant, and $f_d(\xi, \mu_c, T) = (e^{(\xi - \mu_c)/k_B T} + 1)^{-1}$ is the Fermi–Dirac distribution, where k_B is Boltzmann’s constant

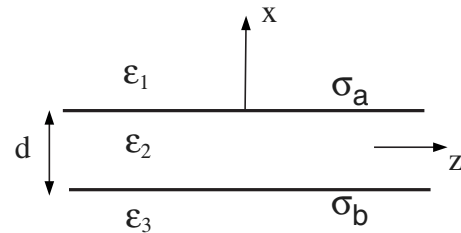


FIG. 1. Graphene PPWG (side view) formed by two graphene sheets, each characterized by surface conductance $\sigma_{a,b}$.

^{a)}Electronic mail: george@uwm.edu.

and T is temperature. The first term in Eq. (1) is due to intraband contributions, and the second term is due to interband contributions. For the cases considered here the intraband term dominates and can be evaluated as

$$\sigma = \sigma_{intra} = -j \frac{e^2 k_B T}{\pi \hbar^2 (\omega - j\tau^{-1})} \times \left[\frac{\mu_c}{k_B T} + 2 \ln(e^{-\mu_c/k_B T} + 1) \right]. \quad (2)$$

Assuming a two-dimensional (laterally infinite) structure consisting of planar layers of isotropic materials with normal along the x -axis, electromagnetic fields can be separated into transverse electric (TE) and transverse magnetic (TM) fields with respect to a lateral coordinate. Here the waveguiding axis is chosen as the z -axis, and from source-free Maxwell's equations the TM^{*c*} fields in each region are

$$\frac{\partial H_y}{\partial z} = -j\omega \varepsilon_i \varepsilon_0 E_x, \quad (3)$$

$$\frac{\partial H_y}{\partial x} = j\omega \varepsilon_i \varepsilon_0 E_z, \quad (4)$$

$$\frac{\partial E_x}{\partial z} - \frac{\partial E_z}{\partial x} = -j\omega \mu_0 H_y, \quad (5)$$

leading to the wave equation

$$\left(\frac{\partial^2}{\partial x^2} + \frac{\partial^2}{\partial z^2} + k_i^2 \right) H_y(x, z) = 0, \quad (6)$$

where $k_i = \sqrt{\varepsilon_i} k_0$, $i = 1, 2, 3$ is the wavenumber in region i , ε_i is the relative permittivity of region i , and $k_0 = \omega \sqrt{\mu_0 \varepsilon_0} = \omega/c$ is the free-space wavenumber (c is the speed of light in vacuum). The boundary conditions to be enforced at material interfaces are

$$\hat{\mathbf{x}} \times (\mathbf{H}_+ - \mathbf{H}_-) = \mathbf{J}^s = \sigma \mathbf{E}, \quad (7)$$

$$\hat{\mathbf{x}} \times (\mathbf{E}_+ - \mathbf{E}_-) = 0, \quad (7)$$

$$\lim_{x \rightarrow \pm\infty} \mathbf{E}, \mathbf{H} = 0, \quad (8)$$

where \mathbf{J}^s (A/m) is an electric surface current on the boundary, \mathbf{E}_+ and \mathbf{H}_+ are the fields on the upper side of the interface, \mathbf{E}_- and \mathbf{H}_- are the corresponding fields on the lower side of the interface, and σ is the interface conductivity (units of S, not S/m). The solution of Eq. (6) can be written as $H_y(x) e^{\pm j\beta z}$, where β is the unknown propagation constant. The resulting dispersion equation for the guided modes is

$$(c_a + c_b) \cos \gamma_2 d + (c_a c_b + 1) j \sin \gamma_2 d = 0, \quad (9)$$

where

$$c_a = \left(\frac{\varepsilon_2 \gamma_1}{\varepsilon_1 \gamma_2} \right) \left(1 + \frac{\sigma_a \gamma_1}{\omega \varepsilon_1 \varepsilon_0} \right)^{-1}, \quad (10)$$

$$c_b = \left(\frac{\varepsilon_2 \gamma_3}{\varepsilon_3 \gamma_2} \right) \left(1 + \frac{\sigma_b \gamma_3}{\omega \varepsilon_3 \varepsilon_0} \right)^{-1}, \quad (11)$$

$\gamma_i^2 = k_i^2 - \beta^2$, and $\text{Im}(\gamma_{1,3}) < 0$. If the dependence on the plate separation vanishes (i.e., when $\sigma_a = 0$ and $\varepsilon_1 = \varepsilon_2$, or $\sigma_b = 0$ and $\varepsilon_2 = \varepsilon_3$), then it is easy to see that $c_a + c_b = c_a c_b + 1$, and Eq. (9) becomes

$$(c_a + c_b) e^{j\gamma_2 d} = 0. \quad (12)$$

In this case, $(c_a + c_b) = 0$ is the dispersion equation for plasmon-polaritons (TM modes) of a single graphene sheet embedded at the interface of two dielectrics, as given in Eq. (37) in Ref. 11. In all other cases, it is convenient to write Eq. (9) as

$$\tan \gamma_2 d = j \frac{c_a + c_b}{c_a c_b + 1}. \quad (13)$$

In the special case of $\sigma_a = \sigma_b = 0$, Eq. (13) reduces to the well-known result for an asymmetric dielectric slab waveguide,²⁰ and, as $\sigma_a, \sigma_b \rightarrow \infty$ the usual perfectly conducting PPWG case is obtained.

Modal fields are

$$H_y(x) = \begin{cases} A e^{-j\gamma_1 x}, & x > d/2 \\ B \sin \gamma_2 x + \cos \gamma_2 x, & -d/2 \leq x \leq d/2 \\ C e^{j\gamma_3 x}, & x < -d/2, \end{cases} \quad (14)$$

where A , B , and C are constants with respect to position.

Excepting the special case Eq. (12), all TM^{*c*} modes can be obtained from Eq. (13). For the quasi-TEM mode of interest here, an approximate solution can be found by assuming that the graphene PPWG is a perturbation of a perfectly conducting PPWG (which would guide a pure TEM mode). The approximations

$$\tan \gamma_2 d \approx \gamma_2 d, \quad \frac{\sigma_a \gamma_1}{\omega \varepsilon_1 \varepsilon_0}, \frac{\sigma_b \gamma_3}{\omega \varepsilon_3 \varepsilon_0} \gg 1$$

lead to

$$\beta/k_0 \approx \sqrt{\varepsilon_2 \left\{ 1 + \frac{1}{\eta_0^2 \sigma_a \sigma_b} \left[\varepsilon_2 - j \frac{(\sigma_a + \sigma_b) \eta_0}{k_0 d} \right] \right\}}. \quad (15)$$

Not surprisingly, the outer dielectric regions play no role if the interface conductivity is sufficiently large. For the simple case of $\varepsilon_2 = 1$ and $\sigma_a = \sigma_b = \sigma$,

$$\beta/k_0 \approx \sqrt{1 - j \frac{2}{\sigma \eta_0 k_0 d}}. \quad (16)$$

The semiclassical approach taken here was used in several previous works^{9,11,12,15,16} and is supported by recent experiments on the optical properties of single and bilayer graphene.¹⁰ Using this approach, in Ref. 11 the optical transmission coefficient of a single suspended monolayer was shown to be $T = (1 + \sigma \eta_0 / 2)^{-1}$. In the optical range the low-temperature conductivity is dominated by the interband term, and for $\Gamma = 0$ and $2|\mu_c| < \hbar \omega$, $\sigma = \pi e^2 / 2\hbar$. Therefore, the transmittance is $|T|^2 \approx 1 - \pi \alpha \approx 97.7\%$, where $\alpha = e^2 \eta_0 / 2\hbar$ is the fine structure constant, which is in excellent agreement with measurements.¹⁰

In addition to (monolayer) graphene walls, an approximate model of a multilayer graphene walled PPWG will also be considered. Multilayer graphene structures have attracted attention for possible electronic applications, and the conductivity of bilayer and multilayer graphene structures has been considered in Refs. 21–24. The zero-temperature minimum conductivity of an N -layer structure has been shown to equal N times the monolayer ($N=1$) conductivity.²¹ In the bilayer case, it was shown that $|T|^2=1-2\pi\alpha f_2(\omega)$ (Ref. 22) and for both $\hbar\omega \gg t_\perp$ and $\hbar\omega \ll t_\perp$, $f_2(\omega) \simeq 1$, where $t_\perp \simeq 0.3$ eV is the interplane hopping parameter. The value of $|T|^2=1-2\pi\alpha \simeq 95.4\%$ for bilayer graphene is in excellent agreement with measurement,¹⁰ and this value is also obtained by assuming $\sigma_{\text{bi}}=2\sigma_{\text{mono}}$ in the semiclassical model.¹¹ In Ref. 10, the result $|T|^2=1-N\pi\alpha$ was shown to hold at least up to $N=4$, and here we assume that $\sigma_{N\text{-layer}}=N\sigma_{\text{mono}}$.

III. RESULTS

The following results are for the quasi-TEM mode of a graphene PPWG. For simplicity, suspended graphene sheets will be assumed ($\epsilon_1=\epsilon_2=\epsilon_3=1$) to avoid any influence of a dielectric substrate (remote phonon scattering,²⁵ opening of a bandgap,²⁶ etc.). The chemical potential of graphene can be varied by doping and/or an applied bias. In this work, except for in Table II the chemical potential is $\mu_c=0.5$ eV, which leads to a large charge density $n \simeq 2 \times 10^{13}$ cm⁻². Since $\mu_c/k_B T \gg 1$ though at least 500 K, for all temperatures of interest the conductivity is

$$\sigma \simeq -j \frac{e^2 \mu_c}{\pi \hbar^2 (\omega - j\tau^{-1})}. \quad (17)$$

Therefore, the following results are only dependent on temperature via the relaxation time τ . The relaxation time depends on a variety of other factors, including the presence of impurities, and for simplicity here we use a constant value of $\tau=5 \times 10^{-13}$ s, in the range of values considered in Ref. 27 and in other works (see, e.g., Ref. 19). This value is also consistent with ballistic transport of approximately 500 nm.

Furthermore, assuming $\mu_c/k_B T \gg 1$, at higher frequencies ($\omega \gg \tau^{-1}$) the only control over the conductivity is via the chemical potential. For lower frequencies ($\omega \ll \tau^{-1}$),

$$\sigma \simeq \frac{e^2 \mu_c \tau}{\pi \hbar^2}, \quad (18)$$

and the conductivity is controlled by the product $\mu_c \tau$. Since τ is affected by the presence of impurities, dielectric substrates, and temperature, and μ_c is affected by an applied bias and doping, many factors contribute to the chemical potential and to the product $\mu_c \tau$. Obviously, for waveguiding applications the conductivity should be as large as possible.

Figure 2 shows the normalized complex phase constant β/k_0 from Eq. (13) for a graphene PPWG with plate separation $d=100$ nm, for frequencies in the GHz/far-infrared range. The upper and lower unlabeled curves are for monolayer walls, the case of multilayer walls ($N=10$) is indicated, and for both monolayer and multilayer wall cases the circles are the approximations [Eq. (16)], showing excellent agreement with the numerical solution of Eq. (13). The monolayer

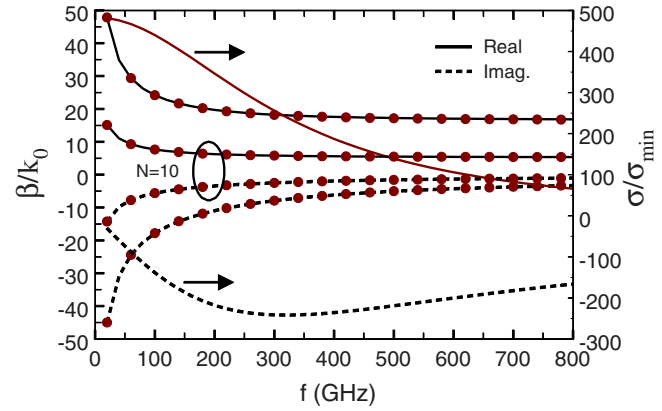


FIG. 2. (Color online) Normalized phase constant β/k_0 from Eq. (13) for a graphene PPWG with $d=100$ nm, having monolayer and multilayer ($N=10$) walls. The monolayer conductivity is normalized by $\sigma_{\text{min}}=\pi e^2/2h$. The approximation [Eq. (16)] is shown as the circles.

conductivity curves are marked with the arrows. It can be seen that throughout most of the considered frequency range, the quasi-TEM mode is relatively nondispersive, even though the conductivity itself is moderately dispersive.

Representative modal fields are shown in Fig. 3 for a graphene PPWG with monolayer walls, $f=100$ GHz and $d=100$ nm (the graphene planes lie at $x=\pm d/2$). The amplitude of the H_y has been set to one since we solve the unforced problem. The E_z component (not shown) is nonzero but is very small compared to the uniform transverse fields in the guide ($E_z/E_x \sim 10^{-3}$), attesting to the quasi-TEM nature of the mode.

To provide a comparison with a metallic structure, a PPWG formed by imperfect ordinary conductors is shown in Fig. 4. Regions 2 and 4 are the metal plates having thicknesses d_2 and d_4 , respectively, and having $\epsilon_2=\epsilon_4=1-j\sigma_{3d}/\omega\epsilon_0$, where σ_{3d} is the frequency-dependent conductivity of the metal plates. Regions 1, 3, and 5 are vacuum with $d_3=d$ and $\epsilon_1=\epsilon_3=\epsilon_5=1$. Assuming gold plates having thicknesses $d_2=d_4=d_m$, two cases are considered in the following: $d_m=10$ and $d_m=100$ nm. The thickness-dependent Drude conductivity σ_{3d} of the gold regions is evaluated from the simplistic Fuchs–Sondheimer model (FS) (Refs. 28–30) and only surface scattering is assumed. In this case, for d_m

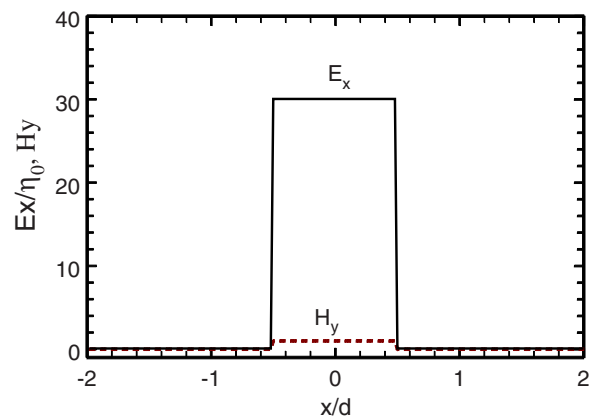


FIG. 3. (Color online) Magnitude of the quasi-TEM modal fields for a graphene PPWG having monolayer walls, $f=100$ GHz, and plate separation $d=100$ nm (the graphene planes lie at $x=\pm d/2$).

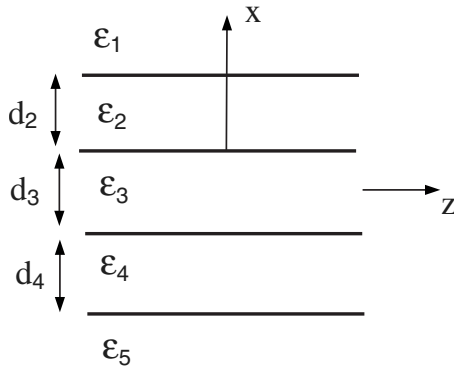


FIG. 4. PPWG formed by imperfect, finite-thickness conductors.

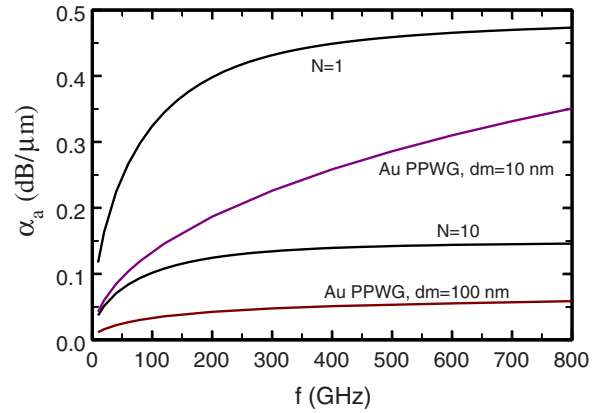
$=10$ nm, $\sigma_{3d}/\sigma_{bulk}=0.57$, and $d_m=100$ nm, $\sigma_{3d}/\sigma_{bulk}=0.93$. In general, grain-boundary scattering and surface roughness would further reduce the effective conductivity, so the results presented here for the metallic waveguide are somewhat optimistic. The dispersion equation for the structure depicted in Fig. 4 is obtained by solving the Helmholtz equation using separation of variables and enforcing the usual boundary conditions of continuous tangential fields. Details are provided in the appendix of Ref. 31.

Table I shows the normalized impedance $Z=|E_x/\eta_0 H_y|$ ($=|\beta/k_0|$) for both graphene mono- and multilayer walled structures and for a gold PPWG for two values of wall thickness. The graphene monolayer case has the highest impedance, the multilayer wall case and the thin gold waveguide have smaller values that are similar to one another (since $\sigma_{3d}d_m \sim \sigma_{multi}$), and the thicker walled gold waveguide has the lowest impedance. Two values of plate separation are considered, and, as expected, the wider plate separation leads to lower impedance.

In Fig. 5, the attenuation $\alpha_a=8.686 \text{ Im}(\beta)$ is shown for the monolayer and multilayer graphene waveguide, as well as for the gold waveguide, for $d=100$ nm. It can be seen that the monolayer case has the highest attenuation, although this can be further decreased by increasing the chemical potential or the product $\mu_c\tau$. Due in part to enhanced surface scattering, the gold waveguide having extremely thin walls ($d_m=10$ nm) has the second-highest attenuation, and grain-boundary scattering or other imperfections could significantly further degrade this result. However, the thinness of the gold walls is the most important factor in determining the attenuation constant of the metal waveguide. For example, at 800 GHz assuming the bulk value of conductivity, the $d_m=10$ nm gold PPWG has only slightly better attenuation (0.295 dB/ μm) compared to the case assuming FS surface

TABLE I. Normalized mode impedance for graphene monolayer, multilayer ($N=10$), and metallic PPWG.

f (GHz)	d (nm)	Z_{mono}	Z_{multi}	Au PPWG $Z_{d_m=10 \text{ nm}}$	Au PPWG $Z_{d_m=100 \text{ nm}}$
100	100	30.1	9.51	10.5	2.91
100	1000	9.55	3.06	3.32	1.17
800	100	17.2	5.50	3.73	1.44
800	1000	5.6	1.97	1.34	1.04

FIG. 5. (Color online) Attenuation $\alpha_a=8.686 \text{ Im}(\beta)$ for $d=100$ nm for the monolayer and multilayer ($N=10$) walled graphene waveguide, as well as for a gold waveguide.

scattering (0.35 dB/ μm). The multilayer graphene waveguide suffers from approximately twice the attenuation of the thicker-walled gold waveguide, but it should be noted that even the $N=10$ multilayer graphene waveguide has wall thickness of only 3 nm. For the graphene structures, considering the infinitesimal wall thickness, both graphene waveguides perform remarkably well.

For plate separation $d=1000$ nm, Fig. 6 shows the attenuation curves. The results are similar to the previous case, although attenuation (and wave impedance) is reduced for all structures because of the wider plate separation. Table II shows attenuation for different values of chemical potential [for $\mu_c=0$ results are given for room temperature using Eq. (17)]. It can be seen that the attenuation can be varied by considerably by changing the chemical potential.

Finally, given the extreme wall thinness of the graphene structure, it is interesting to examine the confinement of the quasi-TEM mode fields. Table III shows the value of the modal field outside the waveguide at $x=2d$, normalized by the field at the center of the guide ($x=0$), where $F=|E_x(2d)/E_x(0)|=|e^{-j\gamma_1 2d}|$ (the designation “multi” indicates the $N=10$ multilayer graphene case). It can be seen that even for the (essentially infinitesimally thin) graphene monolayer

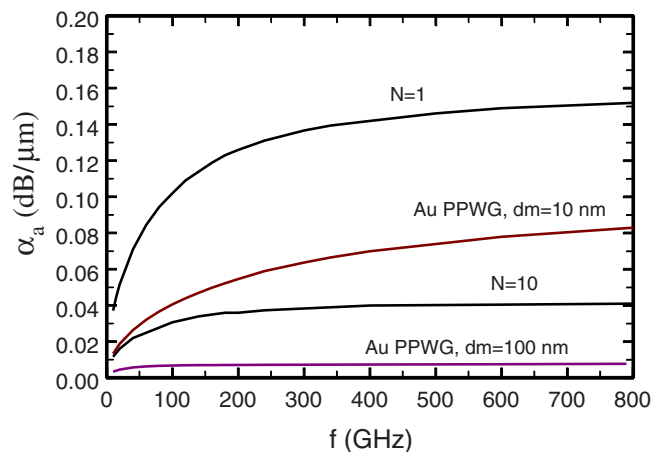
FIG. 6. (Color online) Attenuation $\alpha_a=8.686 \text{ Im}(\beta)$ for $d=1000$ nm for the monolayer and multilayer ($N=10$) walled graphene waveguide, and for a gold waveguide.

TABLE II. Attenuation of a graphene monolayer PPWG, $f=100$ GHz, for different values of chemical potential.

μ_c (eV)	α_a (dB/ μm) $d=100$ nm	α_a (dB/ μm) $d=1000$ nm
0.0	1.220	0.394
0.2	0.513	0.163
0.4	0.362	0.115
0.6	0.296	0.093
0.8	0.256	0.081
1.0	0.229	0.072
1.2	0.209	0.066
1.4	0.193	0.060
2.0	0.162	0.050

wall waveguide, the modal fields outside the waveguide are relatively small and are only approximately an order of magnitude larger than in the case of the much thicker-walled gold waveguide.

IV. CONCLUSIONS

A PPWG formed by graphene walls has been considered. The graphene is represented by an infinitesimally thin, local two-sided conductance surface, and Maxwell's equations were solved for the quasi-TEM model fields guided by the graphene layers. It was shown that a graphene PPWG can guide energy with loss similar to many thicker-walled metal structures. Such waveguides may be competitive with metal structures and can be tuned by varying the chemical potential. Graphene PPWGs may be of interest in electronic and photonic applications.

TABLE III. Modal field value outside the waveguide at $x=2d$, normalized by the field at the center of the guide.

f (GHz)	d (nm)	F^{mono} (10^{-4})	F^{multi} (10^{-4})	Au PPWG $F^{d=10\text{ nm}}$ (10^{-4})	Au PPWG $F^{d=10\text{ nm}}$ (10^{-4})
100	100	31	9.9	8.0	2.8
100	1000	99	31	25	9.1
800	100	138	45	22	6.9
800	1000	404	138	70	22

- ¹A. K. Geim and K. S. Novoselov, *Nature Mater.* **6**, 183 (2007).
- ²K. S. Novoselov, A. K. Geim, S. V. Morozov, D. Jiang, Y. Zhang, S. V. Dubonos, I. V. Grigorieva, and A. A. Firsov, *Science* **306**, 666 (2004).
- ³K. S. Novoselov, A. K. Geim, S. V. Morozov, D. Jiang, M. I. Katsnelson, I. V. Grigorieva, S. V. Dubonos, and A. A. Firsov, *Nature (London)* **438**, 197 (2005).
- ⁴Y. Zhang, J. P. Small, W. V. Pontius, and P. Kim, *Appl. Phys. Lett.* **86**, 073104 (2005).
- ⁵C. Berger, Z. Song, T. Li, X. Li, A. Y. Ogbazghi, R. Feng, Z. Dai, A. N. Marchenkov, E. H. Conrad, P. N. First, and W. A. de Heer, *J. Phys. Chem.* **108**, 19912 (2004).
- ⁶Y. Ouyang, Y. Yoon, J. K. Fodor, and J. Guo, *Appl. Phys. Lett.* **89**, 203107 (2006).
- ⁷A. H. Castro Neto, F. Guinea, N. M. R. Peres, K. S. Novoselov, and A. K. Geim, *Rev. Mod. Phys.* (to be published).
- ⁸V. P. Gusynin, S. G. Sharapov, and J. P. Carbotte, *Phys. Rev. Lett.* **96**, 256802 (2006).
- ⁹S. A. Mikhailov and K. Ziegler, *Phys. Rev. Lett.* **99**, 016803 (2007).
- ¹⁰R. R. Nair, P. Blake, A. N. Grigorenko, K. S. Novoselov, T. J. Booth, T. Stauber, N. M. R. Peres, and A. K. Geim, *Science* **320**, 1308 (2008).
- ¹¹G. W. Hanson, *J. Appl. Phys.* **103**, 064302 (2008).
- ¹²G. W. Hanson, *IEEE Trans. Antennas Propag.* **56**, 747 (2008).
- ¹³S. A. Mikhailov, *Europhys. Lett.* **79**, 27002 (2007).
- ¹⁴V. Ryzhii, A. Satou, and T. Otsuji, *J. Appl. Phys.* **101**, 024509 (2007).
- ¹⁵T. Stauber, N. M. R. Peres, and A. K. Geim, e-print arXiv:0803.1802v3.
- ¹⁶L. A. Falkovsky and S. S. Pershoguba, *Phys. Rev. B* **76**, 153410 (2007).
- ¹⁷G. Y. Slepyan, S. A. Maksimenko, A. Lakhtakia, O. Yevtushenko, and A. V. Gusakov, *Phys. Rev. B* **60**, 17136 (1999).
- ¹⁸M. Dressel and G. Grüner, *Electrodynamics of Solids* (Cambridge University Press, London, 2002).
- ¹⁹V. P. Gusynin, S. G. Sharapov, and J. P. Carbotte, *J. Phys.: Condens. Matter* **19**, 026222 (2007).
- ²⁰D. Marcuse, *Theory of Dielectric Optical Waveguides*, 2nd ed. (Academic, New York, 1991).
- ²¹M. Nakamura and L. Hirasawa, *Phys. Rev. B* **77**, 045429 (2008).
- ²²D. S. Abergel and V. I. Fal'ko, *Phys. Rev. B* **75**, 155430 (2007).
- ²³M. Koshino and T. Ando, *Phys. Rev. B* **77**, 115313 (2008).
- ²⁴A. B. Kuzmenko, E. van Heumen, F. Carbone, and D. van der Marel, *Phys. Rev. Lett.* **100**, 117401 (2008).
- ²⁵S. Fratini and F. Guinea, *Phys. Rev. B* **77**, 195415 (2008).
- ²⁶S. Y. Zhou, G.-H. Gweon, A. V. Fedorov, P. N. First, W. A. de Heer, D.-H. Lee, F. Guinea, A. H. Castro Neto, and A. Lanzara, *Nature Mater.* **6**, 770 (2007).
- ²⁷T. Stauber, N. M. R. Peres, and F. Guinea, *Phys. Rev. B* **76**, 205423 (2007).
- ²⁸K. Fuchs, *Proc. Cambridge Philos. Soc.* **34**, 100 (1938).
- ²⁹E. Sondheimer, *Adv. Phys.* **1**, 1 (1952).
- ³⁰J. Vancea, G. Reiss, and H. Hoffmann, *Phys. Rev. B* **35**, 6435 (1987).
- ³¹G. W. Hanson and A. B. Yakovlev, *Operator Theory for Electromagnetics: An Introduction* (Springer, New York, 2002).